Polymer Nanocomposite Powders and Melt Spun Fibers Filled with Silica Nanoparticles

J. Rottstegge (Y. K. Qiao), X. Zhang, Y. Zhou, D. Xu, C. C. Han, D. Wang

Institute of Chemistry, The Chinese Academy of Sciences, Beijing, Zhongguancun 100080, China

Received 13 March 2006; accepted 24 July 2006
DOI 10.1002/app.25162
Published online in Wiley InterScience (www.interscience.wiley.com).

ABSTRACT: Nanocomposite powders from polypropylene filled with surface modified and unmodified fumed silica have been prepared from polymer solution to achieve improved mixing and have been forwarded to fiber melt spinning. The surface of the fumed silica was modified with dodecyl alkoxy silanes. Crystallization velocity and viscosity of the PP nanocomposites thereof were determined to ensure good melt spinning processing conditions for all composite compositions. Upon addition of untreated filler particles, a shear thinning and an increased crystallization velocity of the polymer melt was found, while only minor changes were detected in the presence of surface modified fumed silica particles. The composites and the polymer fibers made from these powder composites by melt spinning were mainly characterized by optical microscopy (OM), scanning electron microscopy (SEM), mechanical measurements, differential scanning calorimetry (DSC), and solid-state NMR. The unmodified fumed silica was found to have a strong influence on the mechanical fiber properties, while the surface modified silica only a small one. Fibers were additionally characterized with respect to the uniformity, the PP crystallinity, moisture absorption, and the water contact angle. © 2006 Wiley Periodicals, Inc. J Appl Polym Sci 103: 218–227, 2007

Key words: fumed silica; nanocomposites; compatibilization; polypropylene; fibers

INTRODUCTION

Polymer fibers are commonly applied as textiles, carpets, or as additives to reinforce or modify material properties.[1–4] As an additive, they modify bulk polymer properties by blending, they enforce the stability of tires in automobile industry or the flexibility of hardened cement as additive for construction.[5] Already the properties of the fibers themselves depend on their composition and processing conditions.[6] Common melt spun polymer fibers are made from polymers like polypropylene, polyethylene, polyacrylonitrile, polyesters, or polyamides.[1–4] In addition, some fibers are modified by being blended with other polymers[7] or by being compounded with very small amounts of inorganic components,[8] e.g., for dying.

In contrast to the polymer fibers, bulk polymers are easy to be modified by inorganic additives like minerals (e.g., kaolin, quartz), exfoliated layer minerals (montmorillonite nanocomposites), nanofibers (carbon or mineral nanofibers), or by spherical inorganic particles (amorphous Al_2O_3, $CaCO_3$, fumed silica, pigments).[9–11] Despite successful attempts to transfer carbon nanofiber and montmorillonite-modified polymer nanocomposites[12–15] into fibers, difficulties result from particle aggregation, from polymer degradation catalyzed by the additives or from the increased crystallization velocity and polymer crystallinity,[14,16] resulting in brittle fibers. Good processability during the preparation and drawing of composite fibers requires a homogeneous distribution of the filler in the polymer matrix. As a consequence, a high compatibility between the fiber forming polymer and the inorganic filler is generally preferred. A modification of polymer fibers with inorganic fillers by avoiding these problems will give access to a new class of fibers with changed material properties.

While nanosized silica, aluminum oxide, and $CaCO_3$ particles were already used as fillers for polymer compounding[11,17] or as scratch resistant coatings,[18,19] only few papers are published on fibers filled with inorganic particles. Commonly just low amounts of fillers (pigments) are applied for melt spinning. Nevertheless, there are already polymer fibers filled, e.g., with exfoliated montmorillonite[14,15] and carbon nanofibers[12,13] reported in the literature. Problems arise from the weak ionic bonds between the montmorillonite and the applied cationic surfactants (e.g., alkyl ammonium salts[9])/the polymer matrix, which results in partial filler reaggregation during fiber spinning and in a reduced uniformity especially after drawing. Here, surface modified and unmodified silica nanoparticles were applied as fillers within polyolefin nanocomposites and fibers. The compatibility between the different fillers and the polymer matrix and the changes (improvements) in the final fiber properties as obtained by melt spinning due to the filler surface modification were investigated in a more fundamental way.

Correspondence to: J. Rottstegge (joerg.rottstegge@t-online.de).

EXPERIMENTAL

Materials

Both, composites and fibers were mainly made from isotactic polypropylene (iPP) at a molecular weight of $M_w = 193{,}900$ g/mol, a polydispersity of 4.54, and a melt flow index of 15 g/10 min. The melt flow index was adjusted by chemical degradation of the iPP. Fumed silica as filler was provided by Sigma with particle sizes of 7 and 14 nm. Trimethoxy dodecyl silane was taken as surface modifier, *N*,*N* dimethyl benzyl amine as catalyst, and xylene as surfactant for the nanocomposite preparation and the surface modification of the dried fumed silica.

Applied techniques – measurements

Solid-state NMR

Nuclear magnetic resonance (NMR) spectroscopy,[20–22] using the technique of magic angle spinning, (MAS)[21] was applied to acquire the ^{1}H-, ^{13}C-, and ^{29}Si-NMR spectra. The NMR spectra were taken on a Bruker DSX 300 spectrometer, operating at a magnetic field of 7.05 T. All spectra were measured using 4-mm rotors with a commercial double-resonance probe and spinning speeds of 4 to 12 kHz at a temperature of 298 K. The 90° pulse length of all NMR measurements was 5 μs, the recycle delay 2 s (^{1}H-NMR), 20 s (^{13}C DD MAS), and 60 s (^{29}Si-NMR). Spectra were referenced to the resonance frequencies of water, adamantane, and PDMS (^{1}H-, ^{13}C-, and ^{29}Si-NMR). ^{13}C CP MAS experiments were performed by applying a contact time of 2 μs and a recycle delay of 2 s.

Microscopy

The uniformity of the fibers was measured by optical microscopy. Images were taken by a Leica DMLP microscope at 40×, 200×, and 400× using a CCD camera.

The scanning electron microscopy (SEM) images were taken from fiber surfaces and cross sections with a Hitachi S 4300 SEM with platinum sputtering. Samples were fixed to the substrate by means of conductive adhesive tapes. The accelerating voltage of the applied field emission gun was about 15 kV, the working distance about 15 mm applying 500×–20,000×. Fibers for SEM cross sections were embedded in an acrylate agent polymerized at 40°C for 4 days.

Mechanical measurements

The shear viscosity of the composites was determined by an Advanced Capillary Rheometer RH 7 (Flowmaster Series) from Bolin Instruments, applying shear rates of 10 to 3200 1/s and a capillary ($L/D = 32$) of 27 mm length (L). The temperature was set to 200°C in all experiments.

Mechanical measurements of the fibers were performed with an IX automated materials testing system from Instron Corp. The stress was measured as a function of the elongation of a bundle of 48 fibers at an initial length of 10 cm. Elongation was increased at a velocity of 500 mm/min for the undrawn fibers and of 100 mm/min for the drawn ones. From these stress elongation measurements, the maximum stress per area (cN/dtex), the modulus (cN/dtex), the elongation at maximum stress, and the elongation at break were determined. All samples were measured five times, and the results were averaged to obtain a mean.

Water uptake/contact-angle measurements

The water uptake of the fibers was determined after fiber washing to remove traces of the melt spinning additives (e.g., surfactants) from the fiber surface and careful drying for 3 days in vacuum at 70°C. In all cases, the water uptake was determined by weight for 15 g of dried fibers stored for 2 days at 25°C in 100% humidity.

Contact-angle measurements between the composites and a water droplet were monitored by optical microscopy. To get a flat polymer surface, the cleaned composite fibers were molten and quenched on a flat, clean surface from aluminum. A water droplet was put to the resulting plain polymer surface by applying an injection needle. Contact-angle measurements were performed by optical microscopy parallel to the PP surface and were repeated five times. The results were averaged to obtain a mean.

Differential scanning calorimetry

DSC measurements were performed at a PerkinElmer DSC 7 to determine the crystallinity of the polypropylene from the endothermic melting process[16] and the crystallization velocity at isothermal conditions. To prevent further crystallization during the crystallinity measurements of the polypropylene composites, samples of 10.0 mg were treated with the following procedure: Samples were hold for 1 min at 40°C and heated from 40 to 140°C at 200°C/min to avoid additional crystallization at about 120°C. Then heating proceeded at 10°C/min from 140°C to 230°C. The enthalpy of fusion (H_f) was calculated by dividing the endothermic peak area by the weight of polypropylene within the composite sample. Crystallinities (χ_c) of the different composites were obtained by dividing H_f by the extrapolated value of enthalpy corresponding to the melting of 100% crystalline PP of $H_f^0 = 170\,J/g$.[23]

The isothermal crystallization velocities of both, composite and fiber samples, were obtained from these molten samples (after enthalpy of fusion measurements)

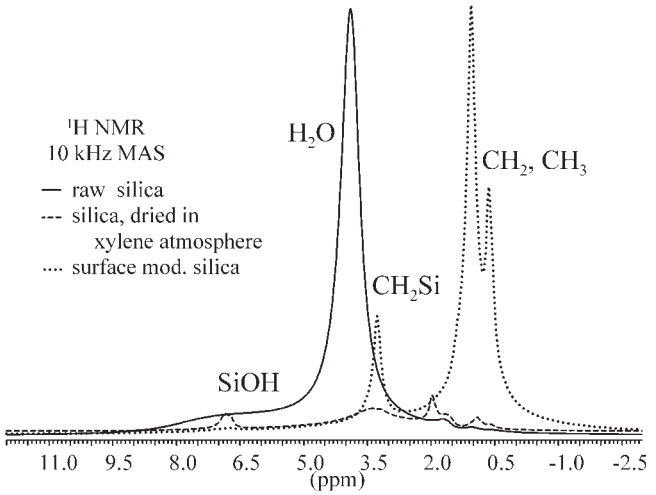

Figure 1 ^{1}H-NMR of nanoparticles before and after drying and surface treatment.

by holding them for another 2 min at 230°C to remove thermal history and by cooling them down to 130°C at 200°C/min. Isothermal crystallization was performed at 130°C. Heat flow and total heat were fitted with respect to the Avrami theory, to determine the heat of fusion, the time constant, the dimension (representing the mechanism and the type of crystal growth), and the time offset.

Composite and fiber preparation

The fumed silica with particle sizes of 7 and 14 nm was initially dried in vacuum at a temperature of 70°C for 3 days. Drying was performed in the presence of traces of xylene to ensure that most of the adsorbed water within the fumed silica (about 10–20 wt %) was either removed or was replaced by xylene. Remaining water could prevent particles from getting well dispersed in the applied low polar solvents and would compete in the grafting reaction of the compatibilizing agent with the silica surface OH groups during the preparation of iPP/fumed silica nanocomposite. The successful drying and surface modification of the fumed silica particles was confirmed by solid-state NMR: In the ^{1}H-NMR spectra of the fumed silica raw material in Figure 1, a strong resonance of remaining water at about 4.0 ppm could be detected. After drying in vacuum by applying a low xylene pressure, this water was almost completely removed and weak signals of absorbed (immobilized) xylene were found.

Each gram of dried fumed silica at a particle size of 7/14 nm for the nanocomposite preparations was then added into 100 g xylene and dispersed by surface treatment with 0.56/0.30 g trimethoxy dodecyl silane as surface modifier and catalytic amounts of *N,N* dimethyl benzyl amine as catalyst. The samples were kept at initially 30, 60, and finally 80°C for several days. After 3 days of stirring and heating, the initial turbid suspensions changed into a clear liquid, showing a good dispersion of the surface modified particles in the xylene. The surface modification was again verified by solid-state NMR as shown in the ^{1}H-NMR spectrum of the dried fumed silica in Figure 1, showing resonances at 0.5–1.2 ppm originating from the grafted alkyl CH_2 and CH_3 groups. ^{13}C DD MAS spectra of the surface-treated silica particles and of the agent for surface modification are shown for comparison in Figure 2. Signals are clearly changed due to the chemical grafting reaction. As a consequence, the NMR spectrum of the highly mobile, liquid trimethoxy dodecyl silane changed to that one of a solid component. The successful surface modification can also be seen in the ^{29}Si-NMR spectra of Figure 3. Most of the fumed silica Q^3 groups having one free OH group were converted into fully saturated Q^4 groups by the silane. To stabilize the dispersed, surface-treated particles, 15.6 g polymer (iPP) was added per 1 g fumed silica to the dispersions and dissolved at 120°C. After 30 min of additional stirring, the clear dispersions were cooled down rapidly. Because of the poor solubility of the applied iPP in xylene at low temperatures, polymer precipitation was very fast. Upon cooling and fast precipitation, the dispersions from silica nanoparticles in the polymer solutions were frozen into polymer filler precipitates. The polymer precipitates/gels were then dried in vacuum for 2 days at a temperature of 30°C and finally for 1 day at 70°C to stabilize the filler distribution in the polymer matrices. Finally, iPP/fumed silica nanocomposite powders were obtained having a (surface modified) filler particle content of 10 wt %. This procedure was applied to all samples, the surface-treated and untreated fumed silica particles of 7 and 14 nm size. If samples without silica surface modification were applied, no clear silica polymer dispersions were finally obtained. Upon addition of the polymer to the unmodified silica xylene suspensions, the carefully stirred, clear dispersions became turbid.

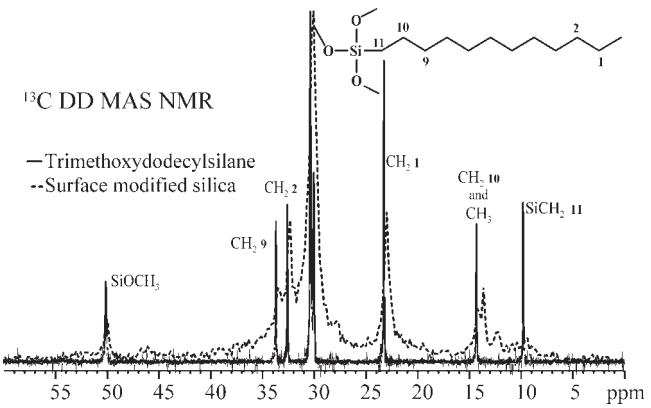

Figure 2 ^{13}C DD MAS NMR of the siloxane before and after particle surface treatment.

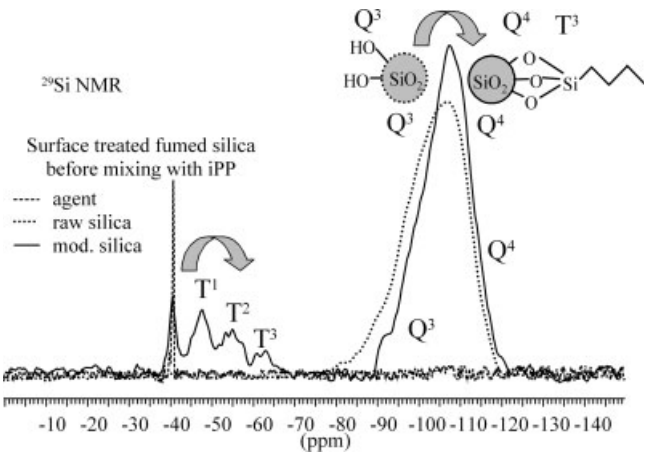

Figure 3 ^{29}Si-NMR of nanoparticles before and after surface treatment.

The remaining unmodified iPP was milled to a powder. Samples for fiber melt spinning at different filler contents were obtained from the iPP/fumed silica nanocomposite powder and the iPP powder by careful mixing before melt mixing and spinning in a melt extruder was performed. iPP composites and the fibers samples thereof filled with 7 nm sized fumed silica were prepared at surface modified fumed silica filler contents of 0, 0.1, 0.2, 0.3, 0.5, 1, 2, 3, 4, and 5 wt %, those iPP composites filled with 7 nm sized fumed silica without surface treatment at concentrations of 0, 0.2, 0.5, and 1 wt %. The corresponding samples of 14 nm sized surface modified and unmodified fumed silica were prepared at filler concentrations of 0, 0.2, 0.5, and 1 wt %. In addition, the samples for differential scanning calorimetry and shear viscosity measurements were initially melt mixed with a single-screw ($L/D = 25$) melt extruder to ensure a good composite mixing for all filler concentrations.

The polymer composites were forwarded to melt spinning. Melt spinning was performed on a single-screw ($L/D = 25$) melt extruder to achieve improved mixing with a spinneret containing 48 orifices, each 0.35 mm in diameter. The extruder was set with five different temperature zones of 200, 220, 230, 235, and 230°C at the feed, metering, melt-blending, die, and spinneret sections, respectively. The as-spun filaments were collected at a take-up speed of 300 m/min and drawn at 110°C on a four-positioned drawing platform to drawing ratios of 3 and 5. Fibers were characterized with respect to their diameter (tex) to be in the range of 57.0 to 58.5 tex (47.1–47.9 μm) for the undrawn fibers, 17.5–18.5 tex (26.2–26.9 μm) for fibers at drawing ratio 3 and 10.9–11.5 tex (20.7–21.2 μm) for the fibers at drawing ratio 5. All the prepared fibers are listed in Table I according to their filler concentration, size and type (surface modified or surface unmodified particles) and the measured fiber diameters at different drawing ratios.

TABLE I
Fiber Diameters (μm) and Errors of iPP Fibers (Filled with Modified and Unmodified 7 and 14 nm Sized Particles) at Different Drawing Ratios as Obtained by Optical Microscopy and Gravimetry

Filler size, surface	Conc. (wt %)	Undrawn		Draw ratio 3		Draw ratio 5	
		Microscopy	Gravimetry	Microscopy	Gravimetry	Microscopy	Gravimetry
7, mod.	0.0	–	47.7	24.6 (1.5)	26.6	20.0 (2.0)	20.9
7, mod.	0.1	–	47.8	–	26.5	–	21.1
7, mod.	0.2	–	47.5	23.6 (1.5)	26.5	21.9 (1.0)	20.7
7, mod.	0.3	–	47.5	25.3 (1.5)	26.7	21.7 (1.5)	20.9
7, mod.	0.5	–	46.7	–	26.3	–	21.1
7, mod.	1.0	–	47.3	24.5 (2.0)	26.5	20.8 (1.0)	21.1
7, mod.	2.0	45.5 (2.0)	47.6	23.3 (1.5)	26.4	19.5 (1.0)	20.9
7, mod.	3.0	–	47.7	25.2 (1.5)	26.6	22.6* (1.5)	20.9
7, mod.	4.0	49.0 (6.3)	47.9	25.4 (2.0)	26.4	20.5 (1.5)	21.2
7, mod.	5.0	–	47.7	24.7 (1.0)	26.6	22.5* (2.0)	20.9
7, unmod.	0.0	48.0 (6.0)	47.5	–	26.5	21.0 (1.5)	20.9
7, unmod.	0.2	–	47.3	–	26.3	–	20.8
7, unmod.	0.5	–	47.5	–	26.2	–	21.0
7, unmod.	1.0	44.6 (4.0)	47.5	25.1 (1.3)	26.2	20.2 (2.2)	20.9
14, mod.	0.0	–	47.4	–	26.7	–	21.1
14, mod.	0.2	–	47.8	–	26.9	–	21.2
14, mod.	0.5	–	47.6	–	26.8	–	21.0
14, mod.	1.0	–	47.3	–	26.6	–	20.9
14, unmod.	0.0	–	47.7	–	26.5	–	20.8
14, unmod.	0.2	–	47.3	–	26.6	–	20.7
14, unmod.	0.5	–	48.1	–	27.0	–	21.0
14, unmod.	1.0	–	47.8	–	27.0	–	20.9

Values inside parentheses are error values.

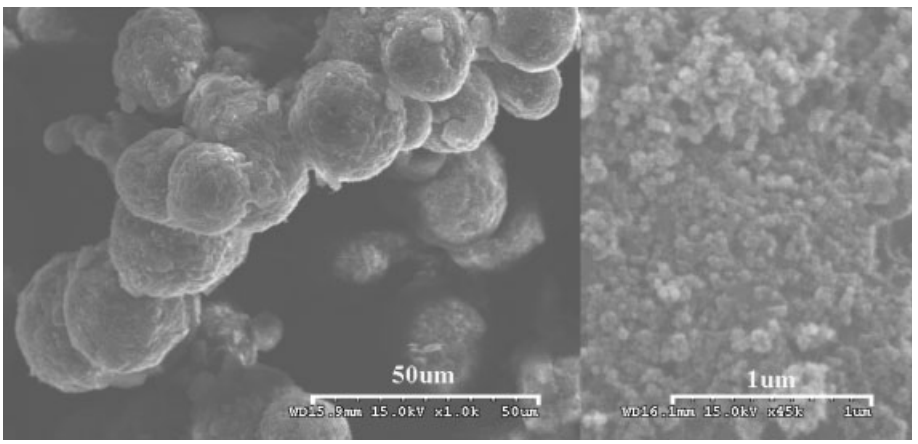

Figure 4 SEM images of the dried composite showing the obtained composite powder in the left image (×500) and a more detailed, fine structure (×22,500) in the right image.

RESULTS AND DISCUSSIONS

The composites

On precipitation and drying, the composite dispersions were converted into powders as displayed in the SEM images of Figure 4. The iPP composite powders consisted of spheres with 10–20 μm size. Each contained multiple 50–200 nm sized sub spheres, consisting of multiple polymer stabilized nanosized filler particles. Similar structures were usually obtained upon spray drying of polymer stabilized redispersible latex dispersions.

To apply appropriate melt spinning conditions for all composite samples, the shear viscosity of the composites was determined at 200°C as shown in Figure 5. Upon addition of 1 wt % unmodified fumed silica particles to the iPP, the melt viscosity was increased for both applied particle sizes of 7 and 14 nm. Findings clearly changed in the presence of surface modified fumed silica (7 and 14 nm size) up to contents of 5 wt %. There were just small differences in the shear viscosity of the iPP composites found, resulting in a weak shear thinning as observed at small shear rates.

These findings are well in accordance with the literature:[17,24,25] With higher filler content, the melt viscosity of high-impact polystyrene/organomontmorillonite nanocomposites[24] and of P(BuMA) $CaCO_3$ composites[17] was recently found to be increased. The polymer viscosity itself was in addition found to be a function of the filler content. Only minor differences in the viscosities were found between pure PP and PP composites filled with ethanol-treated fumed silica.[25]

The crystallization velocity of the iPP composite powders was determined by isothermal crystallization at 130°C after fast quenching of the samples from melt. All data were fitted according to the Avrami theory to determine the crystallization enthalpy and the (primary) crystallization order and kinetics. Trivially, most interesting among the results (as obtained from the Avrami isothermal crystallization parameters) was the dependency of the (fitted) time of maximum crystallization rate (maximum heat flow) as a function of the particle/filler concentration. This is shown for the iPP composites filled with surface coated or unmodified SiO_2 nanoparticles (of 7 and 14 nm size) in Figure 6. Generally, on addition of all the fillers, crystallization was found to be faster. The time of maximum crystallization rate/heat flow was reduced in all cases. Differences between coated/uncoated filler particles were clearly visible: iPP crystallization was already two times faster in the presence of 4 wt % surface modified fumed silica, but it was even faster for the unmodified fumed silica particles. Upon surface coating of the filler particles the iPP composite crystallization velocity was obviously less accelerated. Up to seven times higher contents of surface coated fillers were necessary to obtain the same crystallization velocities as for the uncoated fillers. These massive changes in the crystallization velocity (represented in the time constant) were accompanied by minor differences in the heat of fusion and

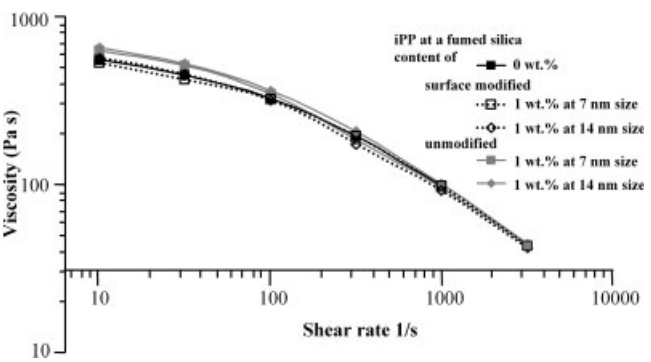

Figure 5 Shear viscosity of iPP composites filled with 1 wt % surface modified and unmodified fumed silica particles of 7 and 14 nm size at 200°C.

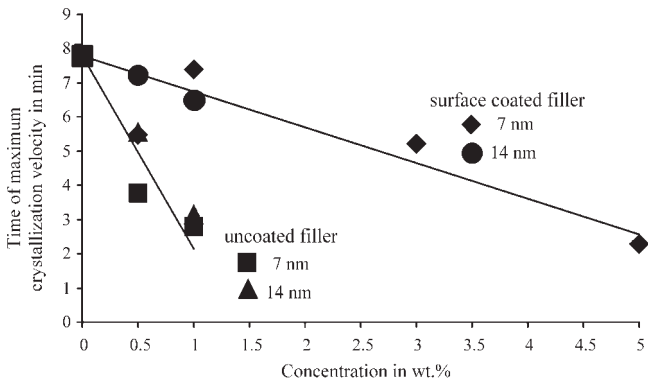

Figure 6 Time t_{max} at maximum crystallization rate v_{max} during the isothermal crystallization of melts from iPP composites filled with surface coated or unmodified SiO_2 nanoparticles (7 and 14 nm) at 130°C.

the dimension, representing the mechanism and the type of crystal growth.

The increase in the crystallization velocity was most probably due to a nucleation of the iPP crystallization by the fumed silica. In all cases, the times of maximum crystallization rate, representing the crystallization velocities, depended linear on the filler concentration. The efficiency of the additional iPP nucleation caused by the filler was clearly reduced by the silica surface coating.

Fibers

Some of the fibers as obtained by melt spinning are shown in the optical micrographs (Fig. 7). In the bottom row of Figure 7, there are optical microscopy images of iPP fibers at a unmodified 7 nm sized fumed silica content of 1 wt % shown. While an undrawn fiber is depicted in the left image, the corresponding fiber at a drawing ratio of 5 is presented in the right image. The uniformity of the fibers was poor in the presence of just 1 wt % of unmodified nanoparticles. Both optical microscopy images in the top row display iPP fibers filled with 2 wt % of 7 nm sized surface modified fumed silica before drawing (left image) and at a draw ratio of 5 (right image). In contrast to the findings on the unmodified fillers, all the obtained composites fibers filled with surface modified nanoparticles show a good uniformity and a smooth surface for all applied concentrations[26] (compare also with Table I).

Within the optical micrographs (transmission mode), the fiber acts as a lens. Fluctuations in the composition and as a consequence in the refractive index greater than or in the range of the wavelength of the applied light will cause optical errors. Besides the limited fiber uniformity in the presence of 1 wt % of the applied unmodified particles, the fiber drawing at a draw ratio of 5 was limited to a very small yield. As to be seen in the optical micrographs of the drawn fibers, several cracks can be found parallel to the direction of the elongation due to poor material properties. In contrast to this, there were generally just small optical errors present if surface modified nanoparticles were applied as filler, which implies that the surface coated fumed silica particles were well dispersed within the polymer matrices.

The fiber surfaces were investigated using SEM with respect to their shape and uniformity as shown in the SEM images of Figure 8. There could be no differences found in the fiber surface shapes of the undrawn iPP fibers including 0.0 and 5.0 wt % 7 nm sized surface modified fumed silica. Even at a drawing ratio of 5, only minor differences could be found between the surfaces of the filled and unfilled fibers. But the fiber shape and uniformity was clearly altered, if the surface unmodified SiO_2 nanoparticles were applied as filler. This can be seen in the SEM images of Figure 9 for iPP fibers filled with 7 nm sized untreated particles at filler concentrations of 1 wt %. In both SEM images (top row), those of the undrawn fibers and those of fibers at a draw ratio 5, fibers were of poor uniformity. These findings are most probably due to filler aggregation. But nevertheless within SEM cross sections as displayed in Figure 9 smooth iPP fiber cross sections could generally be observed, no inhomogeneieties.

Small differences could also be detected in the ^{1}H- and ^{13}C- solid-state NMR spectra of the fibers. While the ^{1}H-NMR spectra of the undrawn fibers at 4 kHz MAS were almost the same for all filler contents (bottom row of Fig. 10), spectra slightly differed after

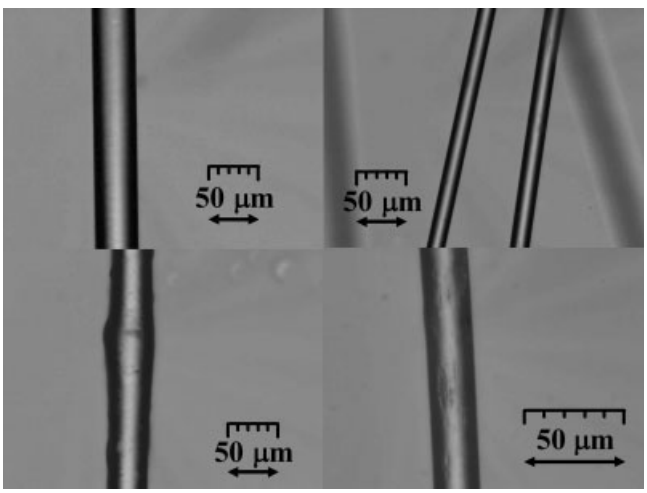

Figure 7 Top row: Optical microscopy image (×200) of an undrawn iPP fiber (left image) at a surface modified fumed silica (7 nm sized) content of 2 wt % and at a draw ratio of 5 (right image). Bottom row: Optical microscopy image (×200 and ×400) of an undrawn iPP fiber (left image) at a unmodified fumed silica (size: 7 nm) content of 1 wt % and at a draw ratio of 5 (right image).

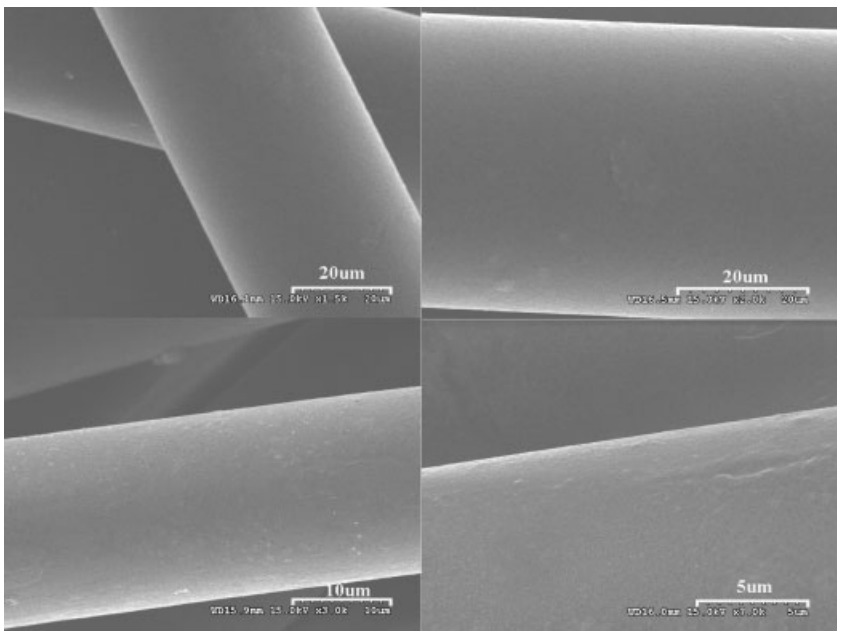

Figure 8 SEM on filled iPP fibers, with 5.0 wt % surface modified fumed silica nanoparticles of 7 nm size: top undrawn iPP fibers (×750 and ×1000), bottom row drawing ratio of 5 (×1500 and ×3500).

drawing as to be seen in the top row. In all cases, the main resonances could be found within the broad signals of the immobile polymer components, nevertheless some components were already resolved in the ^{1}H-NMR spectra at slow MAS with resonance frequencies of 3.5 ppm and between 0 and 2 ppm. While the last ones were due to alkyl chains, those at 3.5 ppm are most probable due to polymer surface OH groups showing a partial oxidation of the iPP during drawing.

Within the ^{13}C- solid-state NMR spectra (CP MAS and DD MAS), there were only small differences found in the relative signal intensities and therefore in the crystallinity as determined by NMR.[27,28] Drawing

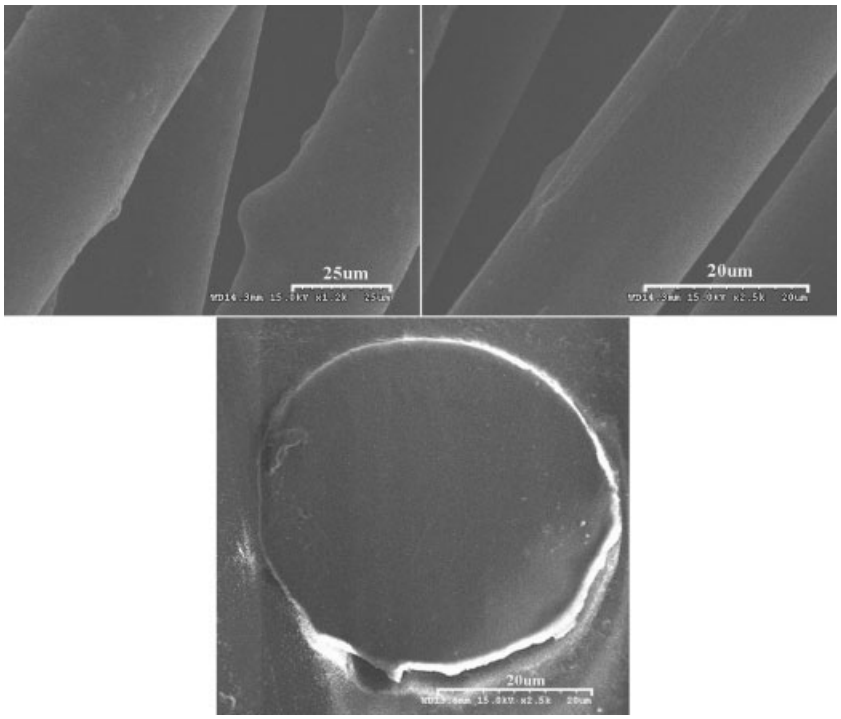

Figure 9 SEM images of iPP fibers filled with untreated SiO_2 nanoparticles (7 nm), at filler concentrations of 1 wt %, left image undrawn fiber, right draw ratio 5, bottom SEM cross sections of the undrawn fiber (×600, ×1250, and ×1250).

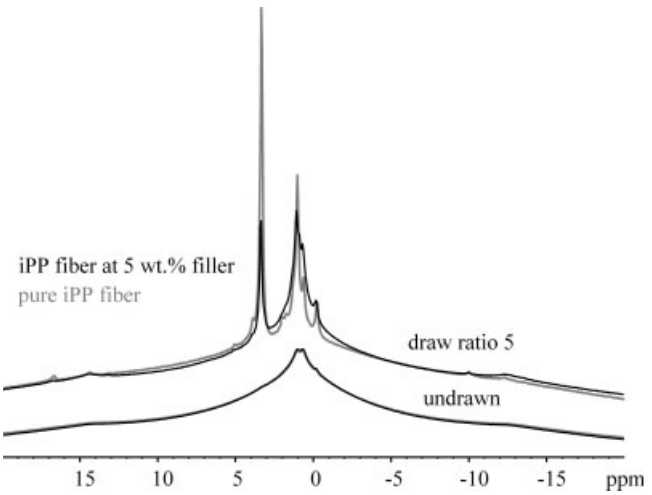

Figure 10 ^{1}H-NMR spectra of undrawn fibers and of fibers at a drawing ratio of 5 (top) at 4 kHz MAS.

changed the relative signal intensities and therefore the crystallinity (and orientation) of the fibers more than the filling with inorganic particles. Nevertheless, the crystallinity seemed to be increased due to the filler but to a smaller extent than on drawing.

The iPP crystallinity within the fibers as determined by DSC is shown in Figure 11 as a function of the filler content, e.g., for fibers at draw ratio 3. Upon increase of the surface modified SiO_2 filler content (7 nm sized), the crystallinity increases slightly up to 55%. Findings were the same upon addition of 14 nm surface modified filler. For unmodified fillers, the initial increase in the crystallinity was stronger. This nicely fits with the results of the crystallization velocities of the composites in Figure 6. Our findings on the increased crystallization velocity and increased crystallinity in iPP/unmodified SiO_2 nanocomposites with higher SiO_2 content as prepared from dispersions in xylene are in agreement with a recent study on melt-mixed nanocomposites.[11] Here, melt-mixed composites from iPP and unmodified/methyl modified commercial fumed silicas were compared. Owing

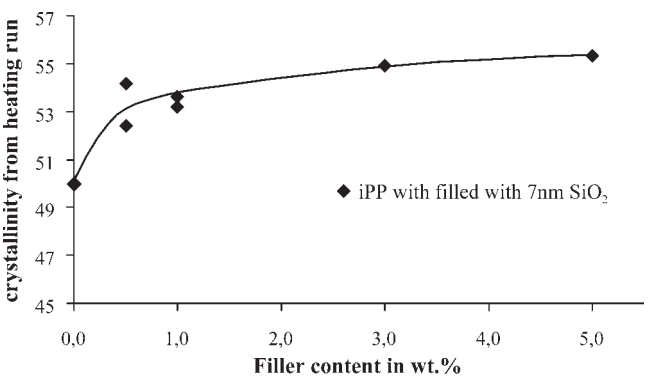

Figure 11 Crystallinity of iPP fibers at draw ratio 3 as determined by DSC.

to the limits of melt mixing, a massive filler aggregation was generally observed. Our data, on the influence of surface modified versus unmodified SiO_2 nanoparticles as fillers for iPP fibers, clearly differ to this study due to the different surface modification (dodecyl alkyl chain versus methyl group) and the sample preparation (solution versus melt mixing). A polymer crystallization inhibition upon addition of the silica as reported for PEO fumed silica composites[29] could not be observed. But our results nicely fit with the crystallinity data of a recent SAXS/WAXD study on melt spun isotactic polypropylene-modified carbon nanofiber nanocomposites.[12]

Mechanical measurements of the fibers differed clearly upon variation of the filler type and content. Measurements were performed on a bundle of 48 iPP fibers filled with different concentrations of surface modified and unmodified fumed silica. Results on the elongation at maximum stress of the iPP fibers filled with surface-coated SiO_2 nanoparticles (7 nm) at filler concentrations of 0–5 wt % were shown in Figure 12. Upon increasing the content of the 7 nm sized surface modified filler, there was only a small decrease in the elongation at maximum stress found. The influence of the surface modified filler to all the mechanical properties—elongation at break, modulus, and maximum stress per area—was also poor.

Findings were different if the dried but unmodified fumed silica particles were applied. In Figure 13, the elongation at maximum stress as part of the mechanical measurements is shown for a bundle of 48 drawn iPP fibers filled with surface modified and unmodified fumed silica nanoparticles of 7 and 14 nm size as a function of the filler concentrations up to 1 wt %. A strong decrease in the elongation at maximum stress of the prepared iPP fibers was found if surface unmodified fillers were applied. In contrast to this, only a small influence of the silica particle size was found

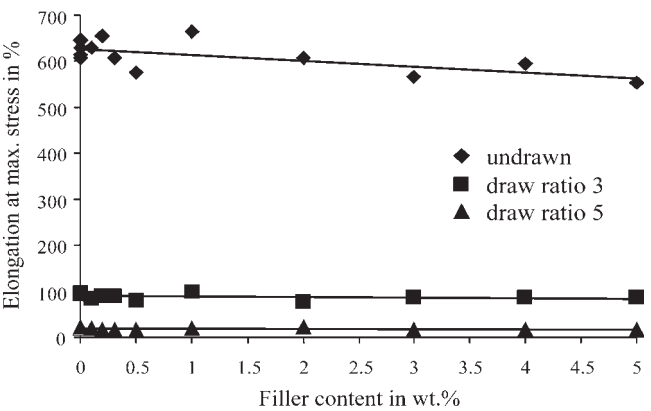

Figure 12 Mechanical measurements on a bundle of 48 iPP fibers filled with surface modified fumed silica. iPP fibers filled with surface coated SiO_2 nanoparticles (7 nm) are shown at filler concentrations of 0, 0.1, 0.2, 0.3, 0.5, 1, 2, 3, 4, and 5 wt %.

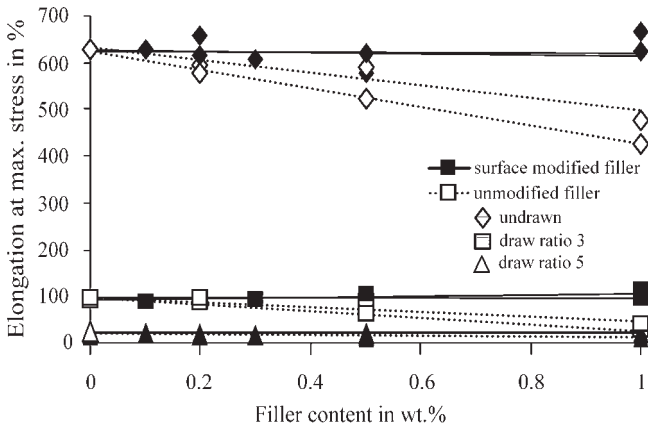

Figure 13 Mechanical measurements on a bundle of 48 drawn iPP fibers filled with surface modified and unmodified fumed silica. Filled symbols represent iPP fibers filled with surface coated SiO_2 nanoparticles (7 and 14 nm) at different filler concentrations, while open ones iPP filled with uncoated SiO_2 nanoparticles (7 and 14 nm) at different filler concentrations.

for both surface modified fillers of 7 and 14 nm size. Findings on the maximum stress per area and on the elongation at break of the prepared iPP composite fibers were similar as for the elongation at maximum stress. The addition of the surface unmodified fillers resulted in a strong decrease in the maximum stress per area and in the elongation at break, while only small differences in the mechanical properties were found for the surface modified fillers (data not shown here). A strong decrease in the iPP fiber modulus could be observed upon addition of the surface unmodified fillers especially at draw ratio 5, but again the change in modulus was poor for the different filler sizes for surface modified fillers. Results on the mechanical measurements imply that the dispersion of the unmodified SiO_2 nanoparticles was quite poor, despite the preparation procedure including the dispersion in iPP by xylene and final melt mixing. Obviously, advanced compatibility and particle dispersion was obtained for the surface-modified particles. Besides filler aggregation, the differences in the mechanical properties of the iPP fibers filled by surface modified or unmodified fumed silica might also be due to the nucleation of the iPP crystallization, especially in the presence of the unmodified filler.

While the mechanical properties were clearly altered, there were only minor differences in the surface properties (water uptake, contact angle) found. Only a weak decrease in the water contact angle to the iPP composite (1° per wt % filler) at high filler loadings and a weak increase of the water uptake was observed but especially the last findings were of the same size as the error.

Finally, an important aspect on nanosized materials is the health issue. But due to recent literature on composites filled with spherical fumed silica,[30] the prepared composites and fibers are expected to be not harmful and not to cause cancer.

CONCLUSIONS

Nanocomposite powders and fibers from polypropylene filled with up to 5 wt % surface modified and unmodified fumed silica have been prepared and characterized. Two different nanosized fumed silica particle types of different size were applied with and without surface modification by trimethoxy dodecyl silane (as a covalently bound coating) for comparison. After solution blending with iPP, precipitation and drying composite powders were obtained. Melt shear viscosity and crystallization velocity of the composites was clearly altered by the unmodified silica particles, but just slightly modified by the alkylated, coated filler. The surface modification (coating) of the filler increased the compatibility between the polymer and the inorganic filler. During melt extrusion and melt spinning, this covalently bound compatibilizing alkyl shell masked the filler and ensured good melt spin and drawing ability resulting in a good fiber quality without defects. For the unmodified filler, the fiber uniformity was poor and drawing became difficult. Nevertheless, the crystallinity of the iPP was found to be increased even in the presence of the coated filler. Mechanical measurements like elongation at maximum stress, elongation at break, the maximum stress per area, and the modulus were strongly altered in the presence of the unmodified fillers, but only slightly modified by the surface modified ones.

The authors acknowledge K. Hou for the NMR measurement time, and Mr. Kuang, T. Meng (all ICCAS), and all the friends who supported this work.

References

1. Schultze-Gebhardt, F.; Herlinger, K. H. In Ullmann's Encyclopedia of Industrial Chemistry; Wiley-VCH: Weinheim, 2002; p 10.
2. Stibal, W.; Schwarz, R.; Kemp, U.; Bender, K.; Weger, F.; Stein, M. In Ullmann's Encyclopedia of Industrial Chemistry; Wiley-VCH: Weinheim, 2002; p 3.
3. Estes, L. L.; Sattler, H.; Berg, H.; Wolf, K. H.; Kausch, M.; Schröer, H.; Pellegrini, A.; Olivieri, P.; Schoene, W.; Nogaj, A.; Sling, C.; Menault, J.; Osugi, T.; Morimoto, O.; Frankenburg, P. E. In Ullmann's Encyclopedia of Industrial Chemistry; Wiley-VCH: Weinheim, 2002; p 6.
4. Elias, H. G. An Introduction to Polymer Science; Wiley-VCH: Weinheim, 1997.
5. Rottstegge, J.; Han, C. C.; Hergeth, W. D. Macromol Mater Eng 2006, 291, 345.
6. Ran, S.; Zong, X.; Fang, D.; Hsiao, B. S.; Chu, B.; Phillips, R. A. Macromolecules 2001, 34, 2569.
7. Utracki, L. A. Commercial Polymer Blends; Chapman & Hall: London, 1998.
8. Marcincin, A. Prog Polym Sci 2002, 27, 853.
9. Ray, S. S.; Okamoto, M. Prog Polym Sci 2003, 28, 1539.
10. Sternstein, S. S.; Zhu, A. J. Macromolecules 2002, 35, 7262.

11. Bikiaris, D. N.; Papageorgiou, G. Z.; Pavlidou, E.; Vouroutzis, N.; Palatzoglou, P.; Karayannidis, G. P. J Appl Polym Sci 2006, 100, 2684.
12. Ran, S.; Burger, C.; Sics, I.; Yoon, K.; Fang, D.; Kim, K.; Avila-Orta, C.; Keum, J.; Chu, B.; Hsiao, B. S.; Cookson, D.; Shultz, D.; Lee, M.; Viccaro, J.; Ohta, Y. Colloid Polym Sci 2004, 282, 802.
13. Sandler, J. K. W.; Pegel, S.; Cadekc, M.; Gojny, F.; van E. M.; Lohmar, J.; Blau, W. J.; Schulte, K.; Windle, A. H.; Shaffer, M. S. P. Polymer 2004, 45, 2001.
14. Zhang, X.; Yang, M.; Zhao, Y.; Zhang, S.; Dong, X.; Liu, X.; Wang, D.; Xu, D. J Appl Polym Sci 2004, 92, 552.
15. Guan, G. H.; Li, C. C.; Zhang, D. J Appl Polym Sci 2005, 95, 1443.
16. Boudenne, A.; Ibos, L.; Fois, M.; Gehin, E.; Majeste, J. C. J Polym Sci Part B: Polym Phys 2004, 42, 722.
17. Chen, J.; Carrot, C.; Chalamet, Y.; Majeste, J. C.; Taha, M. J Appl Polym Sci 2003, 88, 1376.
18. Bauer, F.; Ernst, H.; Decker, U.; Findeisen, M.; Glaesel, H. J.; Langguth, H.; Hartmann, E.; Mehnert, R.; Peuker, C. Macromol Chem Phys 2000, 201, 2654.
19. Glaesel, H. J.; Bauer, F.; Ernst, H.; Findeisen, M.; Hartmann, E.; Langguth, H.; Mehnert, R.; Schubert, R. Macromol Chem Phys 2000, 201, 2765.
20. Ernst, R. R.; Bodenhausen, G.; Wokaun, A. Principles of Nuclear Magnetic Resonance in One and Two Dimensions; Clarendon Press: Oxford, UK, 1986.
21. Schmidt-Rohr, K.; Spiess, H. W. Multidimensional Solid-State NMR and Polymers; Academic Press: London, 1994.
22. Komorowski, R. A. High Resolution NMR Spectroscopy of Synthetic Polymers in Bulk; VCH Publishers: New York, 1986.
23. Chan, C. M.; Wu, J.; Li, J. X.; Cheung, Y. K. Polymer 2002, 43, 2981.
24. Chen, D.; Yang, H.; He, P.; Zhang, W. Compos Sci Technol 2005, 65, 1593.
25. Zhang, L.; Tam, K. C.; Gan, L. H.; Yue, C. Y.; Lam, Y. C.; Hu, X. J Appl Polym Sci 2003, 87, 1484.
26. Qiao, Y. K. (Rottstegge, J.); Zhang, X.; Zhou, Y.; Wang, D.; Xu, D.; Han, C. C. Chin. Pat. Appl. (2005).
27. Saito, S.; Moteki, Y.; Nakagawa, M.; Horii, F.; Kitamaru, R. Macromolecules 1990, 23, 3256.
28. Zheng, C.; Zhang, X.; Rottstegge, J.; Dong, X.; Zhao, Y.; Wang, D.; Zhu, S.; Wang, Z.; Han, C. C.; Xu, D. Chin J Polym Sci, to appear.
29. Ding, J.; Maitra, P.; Wunder, S. L. J Polym Sci Part B: Polym Phys 2003, 41, 1978.
30. Mergeth, R.; Bauer, T.; Kuepper, H. U.; Philippou, S.; Bauer, H. D.; Breitstadt, R.; Bruening, T. Arch Toxicol 2002, 75, 625.